Environmental Science Advances

ROYAL SOCIETY OF CHEMISTRY

PAPER

View Article Online
View Journal | View Issue

Cite this: *Environ. Sci.: Adv.*, 2025, **4**, 1865

Repurposing bauxite residue (a waste material) as an adsorbent for removing PFAS from water

Jingya Pang,[ab] Huixin Qiu,[c] Scott Berggren,[d] Himanshu Tanvar,[e] Brajendra Mishra[e] and Maricor J. Arlos*[ab]

Per- and polyfluoroalkyl substances (PFAS) are synthetic organic compounds characterized by strong C–F bonds and various functional groups, which contribute to their persistence and mobility in the aquatic environment. Bauxite residue (or red mud) is a highly alkaline waste from the aluminum industry, often stored in large quantities in tailing ponds. Recently, growing interest in sustainable waste management has highlighted the potential of bauxite residue to remove organic pollutants from water. This study investigates the use of activated bauxite residue (ABR) (produced *via* a reduction roasting process) as an adsorbent for a mixture of 10 PFAS substances in water. Bench-scale testing demonstrated that long-chain PFAS can be effectively removed by ABR (up to 100%) whereas the short-chain ones achieved 20–100% removal. PFAS removal using ABR follows a pseudo-second-order kinetic model, indicating that chemisorption may play a role during adsorption. This is further supported by the XPS analysis that shows the presence of metal–F bond. Isotherm study further indicated that at its current material characteristics (pore volume = 0.14 $cm^3\ g^{-1}$, BET surface area = 25 g m^{-2}, point of zero charge of ~pH 5), high dosage of ABR (~10 g L^{-1}) is required to reach >85% removal for $\sum$PFAS (n = 10). Cytotoxicity results supported the use of <10 g L^{-1} ABR to minimize ABR toxicity and maximize PFAS removal. Although further material optimization is needed to lower dosage requirements and improve competitiveness with established adsorbents (*e.g.*, powdered activated carbon), our preliminary results highlight the potential of ABR as a promising sorbent for PFAS removal.

Received 14th April 2025
Accepted 19th September 2025

DOI: 10.1039/d5va00101c

rsc.li/esadvances

Environmental significance

Activated bauxite residue (ABR) is a waste material from aluminum industry which can be repurposed as an adsorbent to remove organic pollutants from water (*i.e.*, promoting circular resource use). Here, we assessed the use of ABR to remove a mixture of per- and polyfluoroalkyl substances (PFAS), a diverse group of persistent and bioaccumulative chemicals that are challenging to remediate. We observed that ABR can remove PFAS (especially the long-chain ones) without introducing relevant toxicity by ensuring operation is at neutral pH. This study indicates that ABR is a promising solution to remove PFAS from the water column, offering opportunities to re-use waste materials. Further material improvements and pilot-scale testing are needed to enhance ABR adsorption performance.

1 Introduction

Perfluoroalkyl and polyfluoroalkyl substances (PFAS) have attracted substantial global research interest for several decades.[1] Since the 1940s, PFAS have been incorporated in numerous industrial and consumer products, spanning over 100 sectors.[2,3] Currently, the total annual production of fluoropolymers is estimated at 320 000 tons.[4] Although PFAS are essential components in many products, they are hard to remove from or decompose in the environment[5] due to their amphiphilic and stable characteristics.[6,7] Given their potential to impact human health, many jurisdictions have implemented guidance/regulation for PFAS levels in drinking water.[1,6,8,9] PFAS remain highly recalcitrant to existing wastewater treatment technologies,[10] with precursors transforming into PFAS after biological treatments.[11,12] Adsorption has been regarded as effective for PFAS removal,[13,14] and many conventional and novel adsorbents have been evaluated for their efficiency in removing PFAS from the water column at bench- and pilot-scales.[15–18]

Generated as a by-product from alumina extraction,[19,20] bauxite residue (red mud) has attracted increasing attention in

[a]*Department of Civil and Environmental Engineering, University of Alberta, 9211-116 St. NW, Edmonton, Alberta, T6G 1H9, Canada*
[b]*Department of Civil and Environmental Engineering, University of Waterloo, 200 University Avenue West, Waterloo, Ontario, N2L 3G1, Canada. E-mail: mjarlos@uwaterloo.ca*
[c]*Department of Food Science & Technology, National University of Singapore, 2 Science Drive 2, Singapore 117542, Singapore*
[d]*GRÖN Holding Corporation, 40 King St. West, Suite 5800, Toronto, Ontario, M5H 3S1, Canada*
[e]*Material Science and Engineering, Worcester Polytechnic Institute, Worcester, MA 01609, USA*

waste reuse due to its high abundance, with approximately 1–2.5 tonnes of bauxite residue produced per tonne of alumina[19] and a global generation of ~150 million tonnes per year.[21] This waste material has a low utilization rate (<5% worldwide)[22] mainly due to its potentially hazardous properties, including highly alkaline pH (pH 10–13 (ref. 23)) and risk of metal leaching.[24] Much research has focused on exploiting its recovery and reuse values in construction (bricks, tiles), road aggregates, and pigments.[19,20] Due to its small particle size (diameter of 5–75 μm for about 90% of the particles), high specific surface area and high chemical reactivity,[25] bauxite residue has also been tested as an adsorbent to remove a wide variety of wastewater pollutants such as dyes, phenols, and nutrients.[25–29]

Others have modified bauxite residue to further improve its adsorbent properties (*e.g.*, thermal treatment, acid treatment).[30,31] Using the approach developed by our research team,[32] bauxite residue underwent physiochemical modification *via* a solid-state reduction roasting process, leading to enhanced adsorption capacity and minimal toxic metal leaching potential. This work further demonstrated that this activated bauxite residue (ABR) is capable of removing acid-extractable organics (AEOs) from oil sands process-affected water (OSPW) and other constituents of primary, secondary and tertiary treated municipal wastewater.[28]

The main objective of this study is to evaluate the potential of ABR for removing PFAS from water. The ABR properties were first characterized using several material characterization techniques to gain insights into its adsorption behaviour. A series of bench-scale experiments were then completed to evaluate its performance (adsorption kinetics and isotherms) in removing 11 PFAS (long/short-chain, sulfonic/carboxylic) in environmentally relevant mixtures. Given the potential for ABR to introduce toxicity, cytotoxicity was monitored throughout the experiments to assess potential mitigation options should it be found to contribute to toxicity. The performance of ABR was compared with a commercially available powdered activated carbon (PAC) as a benchmark of ABR's treatment efficiency.

2 Material and methods

2.1 Sample collection and materials

PFAS mixture preparation procedures are detailed in SI-A. The commercially available powdered activated carbon (PAC) was purchased from ClearTech, Canada. Hydrochloric acid (37%), sodium hydroxide (10 N), methanol (≥99.9%), 3,5-dichlorophenol (99%), and ethanol (70%) were purchased from Fisher Scientific, Canada. Ethyl acetate (≥99.5%) and all the PFAS substances were purchased from Sigma-Aldrich, Canada. Ultrapure water was obtained from a MilliQ IQ 7000 purification system with a resistivity of 18.2 MΩ cm (25 °C) and total organic carbon (TOC) ≤5 ppb. Information on bioassay reagents is reported elsewhere.[33] PFAS substances used are listed in Table 1.

2.2 ABR material sample preparation for material characterization

Separate from batch adsorption experiments (Section 2.3), spent ABR material (post-treatment) was characterized to confirm the presence of PFAS and assess changes in ABR characteristics after adsorption. In this experiment, the solution containing ABR and PFAS was mixed on a tube roller (Globe Scientific GTR-AVS Tube Roller) in 50 mL glass centrifuge tubes at 70 rpm for 3 hours. After centrifuging for 5 min at 300 rpm, the supernatant was discarded, and the spent ABR sludge was completely dried at room temperature. The dried, spent ABR samples were collected and stored at room temperature until material characterization.

The porosity of ABR was investigated through the Brunauer–Emmett–Teller (BET) surface area test using the AS-iQ-MP-XR (Anton-Paar GmbH) based on the adsorption and desorption curves of N_2 gas. Before exposing the sample to N_2 at 77 K, virgin and spent ABR were outgassed for 4 h at 200 and 170 °C, respectively. During the BET test, ABR was oversaturated with two long-chain PFAS (PFNA and 6 : 2 PTSA) representative of carboxylic and sulfonic PFAS. The elemental composition and mapping were obtained using the energy-dispersive X-ray (EDX) analysis at 20 kV (Zeiss Sigma FeSEM) with ABR sample affixed to stubs by carbon tapes. The element concentrations and specific atomic structures on the ABR surface were determined by X-ray photoelectron spectroscopy (XPS) (Kratos Axis Ultra spectrometer). ABR samples were also sent to the University of Calgary (Research Instrumentation and Technical Support Lab) for zeta potential measurements to determine the surface charge. Since our batch experiments utilized environmental concentrations that are typically lower (0.5–100 μg L^{-1}), the PFAS adsorbed on the ABR surface could not be clearly observed by material characterization techniques. Hence, our characterization experiments utilized high concentrations of PFAS (100 mg L^{-1}) (Table 1). Other ABR specifications including purity, specific gravity and density are found in SI-B.

2.3 Batch adsorption experiments

Environmental and wastewater concentrations of PFAS ranged from a few ng L^{-1} to ~100 μg L^{-1};[5] hence, our batch adsorption experiments utilized concentrations within this range. A mixture of 10 PFAS in ultrapure water (600 ng L^{-1} each) was first combined with six different dosages of ABR (0, 10, 15, 25, 50, 100 g L^{-1}) at 120 rpm for 24 h using the jar tester (VELP FC 4S Flocculation Stirrer). To assess the impact of adsorption time, two different dosages of ABR (50 and 100 g L^{-1}) were mixed with the same PFAS wastewater at 120 rpm for 1 h and 24 h, respectively. Finally, two different concentrations of PFAS (500 ng L^{-1} and 100 μg L^{-1}) wastewater were treated with 0.1 g L^{-1} PAC, 0.1 g L^{-1} ABR and 10 g L^{-1} ABR at 120 rpm for 24 h. At the end of each experiment, the solution was neutralized using hydrochloric acid to a neutral pH range (6 to 8) and left to settle for 30 to 60 minutes. According to Cheng *et al.*,[28] neutralization of ABR solution is necessary to reduce the leaching of toxic metals (including dissolved Al, Fe, Cr, and V) and also meet many effluent discharge standards for pH. The supernatant was collected and filtered with 1 μm glass fibre filters and then sent to an accredited laboratory for PFAS analysis (completed using the US EPA 1633 method for PFAS analysis by LC-MS/MS) (Bureau Veritas North America).

Table 1 Names and properties of PFAS used in this study. The reported detection limits (RDLs) of all the compounds varied from 0.02–2 μg L^{-1}, depending on the concentration and volume of the sample. pK_a and solubility were obtained from Chemicalize. Abb = abbreviation; MW = molecular weight; pK_a = negative logarithm of the acid dissociation constant (K_a)

Full name – short (S) or long (L) chain	Abb	Chemical formula	MW (g mol^{-1})	pK_a (strongest)	Solubility (pH = 7) (g L^{-1})	Concentration applied
Perfluorobutanoic – S	PFBA	$C_4HF_7O_2$	214.04	0.37	214.039	500 ng L^{-1}[a], 600 ng L^{-1}[b], 100 μg L^{-1}[c,d,e,f], 100 mg L^{-1}[c,g]
Perfluoropentanoic – S	PFPeA	$C_5HF_9O_2$	264.05	0.34	264.047	500 ng L^{-1}[a], 600 ng L^{-1}[b], 100 μg L^{-1}[c,d,e,f], 100 mg L^{-1}[c,g]
Perfluorohexanoic – S	PFHxA	$C_6HF_{11}O_2$	314.05	0.32	314.05	500 ng L^{-1}[a], 600 ng L^{-1}[b], 100 μg L^{-1}[c,d,e,f], 100 mg L^{-1}[c,g]
Perfluoroheptanoic – S	PFHpA	$C_7HF_{13}O_2$	364.06	0.31	364.062	500 ng L^{-1}[a], 600 ng L^{-1}[b], 100 μg L^{-1}[c,d,e,f], 100 mg L^{-1}[c,g]
Perfluorooctanoic – L	PFOA	$C_8HF_{15}O_2$	414.07	0.30	414.07	500 ng L^{-1}[a], 600 ng L^{-1}[b], 100 μg L^{-1}[c,d,e,f], 100 mg L^{-1}[c,g]
Perfluorononanoic – L	PFNA	$C_9HF_{17}O_2$	464.08	0.29	262.6829	500 ng L^{-1}[a], 600 ng L^{-1}[b], 100 μg L^{-1}[c,d,e,f], 100 mg L^{-1}[c,g,h]
Perfluorodecanoic – L	PFDA	$C_{10}HF_{19}O_2$	514.08	0.4	44.521	500 ng L^{-1}[a], 600 ng L^{-1}[b], 100 μg L^{-1}[c,d,e,f], 100 mg L^{-1}[c,g]
Perfluoroundecanoic – L	PFUnA	$C_{11}HF_{21}O_2$	564.09	0.4	10.3686	500 ng L^{-1}[a], 600 ng L^{-1}[b], 100 μg L^{-1}[c,d,e,f], 100 mg L^{-1}[c,g]
Perfluorotetradecanoic – L	PFTEDA	$C_{14}HF_{27}O_2$	714.11	0.4	0.2194	500 ng L^{-1}[a], 600 ng L^{-1}[b], 100 μg L^{-1}[c,d,e,f], 100 mg L^{-1}[c,g]
Perfluorobutanesulfonic – S	PFBS	$C_4HF_9O_3S$	300.1	−3.31	300.09	500 ng L^{-1}[a], 600 ng L^{-1}[b], 100 μg L^{-1}[c,d,e,f], 100 mg L^{-1}[c,g]
6 : 2 Fluorotelomer sulfonic – L	6 : 2 PTSA	$C_8H_5F_{13}O_3S$	428.16	−2.72	428.16	100 mg L^{-1}[h]

[a] Use in the following experiments: removal efficiency of powdered activated carbon (PAC). [b] Removal efficiency at different dosages and exposure duration. [c] XPS. [d] Zeta potential. [e] Adsorption kinetics and isotherm. [f] Cytotoxicity test. [g] EDX. [h] BET surface area analysis.

Given the exploratory nature of this study, a single replication and corresponding recovery studies was used to assess the feasibility of using ABR for PFAS removal. Data derived here will direct studies on optimal conditions for future studies with more controlled replication. Limitations in sample volumes required for chemical analyses also contribute to this decision. Error bars were representative of ±20% measurement uncertainty and were adopted to represent typical variability in analytical measurements.

2.4 Adsorption kinetics and isotherm

Using the information (adsorption duration) derived from Section 2.3, the kinetic experiments were completed by mixing 400 mL of PFAS wastewater containing 100 μg L^{-1} each PFAS with 50 g L^{-1} ABR at 120 rpm using the jar tester. Samples were collected at 0, 5, 10, 20, 30, 45, 60 and 120 minutes, neutralized, filtered and sent for analysis as before. Note QA/QC controls were also included, consisting of a blank (ultrapure water only) and control containing only PFAS (*i.e.*, 0 g L^{-1} ABR). The data were fit to (1) pseudo-first-order, (2) pseudo-second-order, (3) Weber's intraparticle diffusion, and (4) Elovich kinetic models.

The adsorption isotherm experiments were conducted by mixing different dosages of ABR (0, 0.1, 0.5, 1, 5, 10 g L^{-1}) with 200 mL 100 μg L^{-1} PFAS solution at 120 pm using the jar tester for 24 hours. All the samples were then prepared and analyzed as previously. The data were fit to (1) Langmuir (one of the widely used adsorption isotherm models, assuming homogenous surface and monolayer, reversible adsorption), (2) Freundlich (suggesting a multilayer adsorption process on a heterogeneous surface), (3) Redlich Peterson and Langmuir-Freundlich (Sips) (an empirical model combining Langmuir and Freundlich approaches), and (4) Toth models (an extension of Langmuir model to describe a heterogenous surface and more widely used as a supplement). All the equations are described in SI-C.

2.5 Cytotoxicity analysis

The SPE was conducted for *in vitro* bioassays and the procedure was adapted from[28] with slight modifications. Briefly, Oasis HLB SPE cartridges (6cc/500 mg, Waters Corporation) were preconditioned with 5 mL of methanol followed by 10 mL ultrapure water. Then, water samples were introduced into the cartridges under vacuum. After this, the cartridges were rinsed with 10 mL ultrapure water, then dried under vacuum for 45–60 min. Following drying, the cartridges were eluted with 5 mL methanol and then 5 mL 1 : 1 methanol : ethyl acetate (v/v) by gravity. The eluates were collected and evaporated to complete dryness in a water bath at 35–40 °C with a gentle blow of nitrogen. The dried extracts were then reconstituted in methanol to reach an extraction factor of 1000 (SI-C), then transferred into 2 mL amber vials and stored with parafilm at −20 °C until *in vitro* bioassay analysis.

The determination of cytotoxicity utilized the same reagents, data analysis, and procedure with slight modifications as.[33] Briefly, cytotoxicity was determined by the percent inhibition of *Aliivibrio fischeri* bacteria after exposure to the samples using

the BioTox LumoPlate kit (Environmental Bio-detection Product Inc). The concentration that could cause 10% light inhibition of exposure after 15 minutes ($IC_{10,15min}$) was determined and represented as $1/IC_{10}$ in this study.

3 Results and discussion

3.1 Material characterization

The BET surface analysis showed minimal changes in the surface area of both virgin (25.3 $m^2 g^{-1}$) and spent ABR (25.1 $m^2 g^{-1}$), even after exposure to relatively high concentrations of perfluorononanoic acid (PFNA) and 6 : 2 fluorotelomer sulfonic acid (6 : 2-FTSA) (100 mg L^{-1} each). This result suggests that a substantial portion of the ABR surface area remains available for further sorption. The density functional theory (DFT) pore size distribution also indicates the heterogeneity in ABR pore sizes (Fig. 1a), which enhances its ability to adsorb a wide range of substances, especially PFAS with their varied molecular sizes. Molecules are preferentially adsorbed into pores that closely match their size, as this increases the number of interactions between the adsorbate (*i.e.*, pollutants) and the adsorbent. According to the adsorption free energy concept, as the number of contact points between the adsorbates and the adsorbent's surface increases, adsorption becomes more favorable. This is because multiple contact points along the pore walls create stronger attractive forces compared to adsorption on a two-dimensional surface.[34]

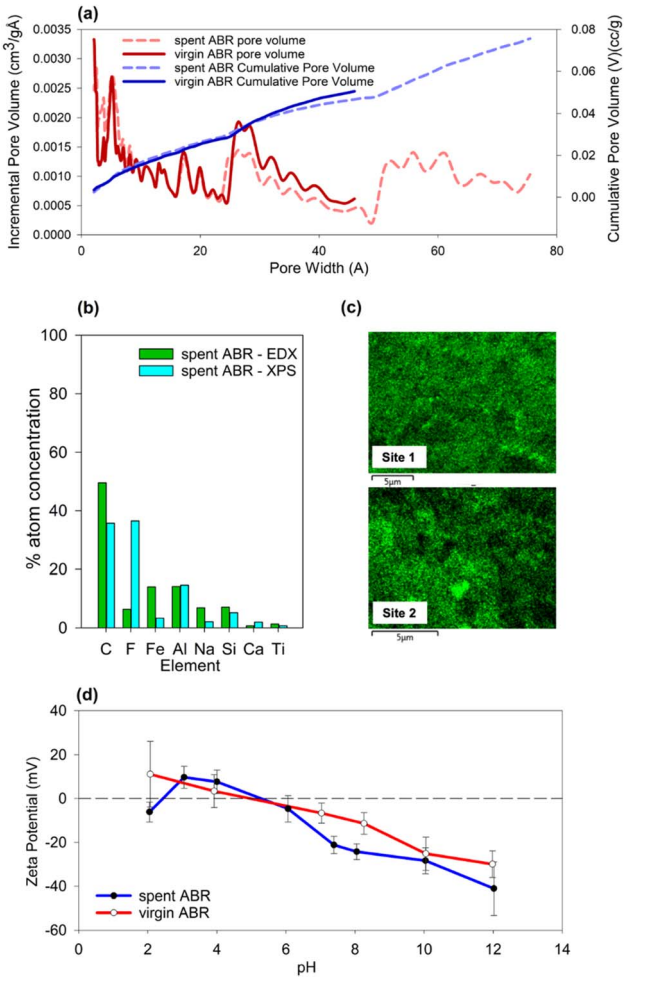

Fig. 1 (a) Pore size distribution obtained *via* density functional theory (Autosorb) of virgin and spent ABR. (b) Comparison of element relative mass by atom for spent ABR between EDX and XPS analyses that measure elemental composition at different depths. (c) Distribution mapping of fluorine (F) on the spent ABR surface from two random sites – higher intensities (green) showing higher concentrations of F. (d) Zeta potential measurements for virgin and spent ABR with a pH correspond to 0 mV as the material's point-of-zero-charge.

The pore size distribution additionally suggests that ABR predominantly contains mesopores (pore diameter between 2 and 50 nm (ref. 35)), which can be further advantageous for PFAS adsorption. Punyapalakul *et al.* observed a faster adsorption rate of PFOA and PFOS on mesoporous adsorbents than microporous ones (pore diameter <2 nm), with interparticle diffusion being the primary adsorption mechanism.[36] Additionally, meso- and macroporous adsorbents were shown to have higher adsorption capacity for long-chain PFAS as larger molecules can easily access adsorption sites and avoid pore blockage.[37] Also, larger PFAS molecules have a preference to aggregate in bigger structures, which leads to a higher removal *via* adsorption.[2] Note that in terms of total pore volume, ABR is better than raw bauxite residues reported in the literature but incomparable to activated carbon-based adsorbents (Table S2). However, while activated carbon has a larger surface area than ABR, it is predominantly microporous, which may be limited for adsorbing smaller molecules.[38]

Although the surface area was unchanged, there were small differences observed between the total pore volumes of virgin and spent ABR, with virgin ABR pore sizes ranging from 2–46 nm and spent ABR with 2–76 nm. This observation indicates that PFAS may have filled or blocked the pores.[34] This result is further supported by XPS and EDX analysis, which detected the presence of fluorine atoms (F) on the surface when ABR was exposed to a mixture of 10 PFAS (100 mg L^{-1} each) (Fig. 1b). Although XPS and EDX provided different relative atom contributions, both analyses were able to detect F, strongly indicating PFAS adsorption by ABR. The main difference in the approaches is their analysis depth, with XPS being more surface-sensitive than EDX. More specifically, XPS is minimally destructive and typically probes the top 1–10 nm of a sample, with elemental sensitivity in the order of 0.1 atomic percent.[39,40] Therefore, XPS is ideal for the analysis of surface chemistry, thin films, and surface adsorption. By contrast, EDX provides information over a larger volume compared to XPS. It can assess relative atom contribution in samples ranging from 1 μm to a few μms (up to 5000 nm) and analyze the bulk material at an analysis depth of 100–3000 nm.[41,42] Therefore, XPS analysis showed relatively higher concentrations of F atoms which are mostly present on the ABR surface.

XPS analysis further revealed the high atom contribution of metallic elements (Al, Na, Fe, Table 2) at low PFAS concentration (0.1 mg L^{-1} PFAS). This result was expected given that the bulk ABR primarily consists of metallic oxides (*e.g.*, Fe_2O_3, Al_2O_3, SiO_2).[28] However, F was at levels higher than the background (*i.e.*, virgin ABR), indicating adsorption of PFAS when added

Table 2 Relative atom concentrations detected by XPS for selected elements on the surface of ABR at different PFAS initial concentrations and ABR dosages. Virgin ABR = 0 g L^{-1} PFAS. PFAS mixture includes PFBA, PFPeA, PFHxA, PFHpA, PFOA, PFNA, PFDA, PFUnA, PFTEDA, PFBS at a concentration of either 0.1 mg L^{-1} (ΣPFAS = 1 mg L^{-1}) and 100 mg L^{-1} (ΣPFAS = 1000 mg L^{-1}). N/A = not applicable. Carbon was analyzed but excluded from the relative atom concentration because as a potential artifact of XPS analysis (use of carbon tape) (Table S3)

PFAS conc	Virgin ABR	0.1 mg L^{-1}			100 mg L^{-1}
ABR dose	N/A	2 g L^{-1}	6 g L^{-1}	10 g L^{-1}	3 g L^{-1}
F	1.37	4.60	2.00	2.07	57.69
Na	22.17	20.54	20.63	21.45	2.97
Fe	19.65	18.05	17.78	19.09	4.88
Ti	2.31	2.13	2.17	2.21	1.11
Ca	4.73	4.42	5.10	5.31	3.01
Si	16.18	15.41	16.86	15.50	7.88
Al	33.60	34.86	35.46	34.36	22.46

into the mixture. To further investigate PFAS sorption, the PFAS concentration was increased 1000-fold (100 mg L^{-1} each PFAS) in 3 g L^{-1} ABR (Table 2). At this high PFAS concentration, the relative atom contribution shifted to ~58% F, confirming that ABR treatment facilitated PFAS removal from the water column and its subsequent adsorption onto the ABR surface.

XPS analyses further provided detailed spectra of each element, allowing for qualitative identification of F-bond types. This feature is particularly useful as it identifies whether C–F bonds are present or if F interacts with other surface elements (*i.e.*, metal–F bonds). No C–F or metal–F bonds were observed on virgin ABR (Table 3). Although the F relative concentration is low (4.6%) for 0.1 mg L^{-1} PFAS concentrations (Table 2), both C–F and metal–F bonds were detected (Table 3). The presence of C–F was expected (*i.e.*, main PFAS bond), but the appearance of metal–F bonds in the spectra suggests that F may interact with other metallic elements on the surface. Given the diverse elemental composition of ABR,[28] it can prove to be a distinct advantage over other emerging adsorbents as it allows additional surficial interactions for diverse types of adsorbates.

When ABR was further oversaturated with 100 mg L^{-1} PFAS (ΣPFAS = 1 g L^{-1}), the C–F bond was more visible while the metal–F bond was no longer observed (Table 3). The result suggests that at high PFAS concentrations, C–F bonding (likely through physisorption) is more favourable than chemical bonding with surficial elements. As a preliminary experiment to determine whether C–F bonds remain after thermal treatment, XPS analysis of thermally treated (550 °C) spent ABR revealed only metal–F bonds (Table 3), suggesting that the thermal treatment can break C–F bonds on the surface. Although some bonds can be broken down at this temperature, complete thermal degradation of PFAS can be accomplished when heated at elevated temperatures (>1000 °C), providing a potential pathway for adsorbent regeneration.[43] Note that evaluating the regeneration and reuse potential of spent ABR is beyond the scope of this study but is an avenue that can be explored further.

SEM and EDX analyses were also completed for spent ABR (exposed to 100 mg L^{-1} PFAS, ΣPFAS = 1 g L^{-1}) to map the distribution of F from two random sites on the surface. The results show that F is present across the surface, though not uniformly distributed (Fig. 1c). Some areas exhibit higher concentrations of F atoms, indicating that these sites may be more conducive to PFAS adsorption. While it is challenging to correlate F elemental map with those of other abundant elemental maps such as C, Fe, Al, Si, Ti, and Na (Fig. S2), the findings nonetheless reiterate the surface heterogeneity of ABR, which can enhance its ability for adsorbing for a wide variety of substances ranging from inorganic anions (*e.g.*, nitrate, fluoride, phosphate), oxides (sulphur, nitrogen, carbon), metal (*e.g.*, arsenic, chromium, nickel, copper, cadmium), and other organic substances (phenols, dyes, acid extractable organics in oil sands processed water) as already observed by others.[26,28]

The zeta potential measurements of ABR at various pH conditions show the surface charge properties of virgin and spent ABR (Fig. 1d). The point of zero charge (PZC) (at which equal numbers of positive and negative charges are present on the surface) is determined to be at ~ pH 5 (Fig. 1d). Also, the surface charge decreased with increasing pH (11.1 mV to −30 mV), suggesting stronger electrostatic repulsion by negatively charged substances at higher pH conditions, which makes ABR adsorption less favourable for these substances. The PZC of spent ABR was observed at ~ pH 6, and with zeta potentials more negative than the virgin ABR. This shift was expected as PFAS exist as anions in the water column, and their adsorption onto ABR may have led to a negative net charge on the surface. At higher pH, the ABR surface charge becomes more negative, leading to stronger electrostatic repulsion (*i.e.*, weaker attractions) with anionic PFAS.[2] Therefore, it is beneficial for ABR to be operated at pH near its PZC, where electrostatic interactions are more favorable (acidic pH conditions are generally avoided, as pH is typically maintained in neutral to mildly alkaline conditions for further treatment or discharge of wastewater). Cheng *et al.* evaluated the leaching of aluminum ions at different pH levels from ABR and found that a pH range of 7–8 reduces aluminum leaching from ABR.[28] This pH range also

Table 3 Fluorine bond types tested from XPS spectra on the surface of ABR at different PFAS concentrations. Bond energy spectra for C–F and metal–F bonds are found in SI (Fig. S1). *The spent ABR was additionally thermally treated at 550 °C for 2 h. N/A = not applicable

ABR dose (g L^{-1})	PFAS conc (mg L^{-1})	Fluorine bond energy position (eV)	Bond type detected
0	0	N/A	N/A
100	0.1	685.0, 688.5	Metal bond, carbon bond
	0.1*	685.5	Metal bond
3	100	688.93	Carbon bond

corresponds to a less negative charge on the ABR surface, which may be more amenable for PFAS adsorption on the ABR surface. Therefore, the bench-scale batch experiments described subsequently below were completed at this pH to reduce the leaching of metallic ions from ABR while maximizing the adsorption of PFAS.

3.2 Adsorption of PFAS mixture by ABR

ABR treatment resulted in good removals of ∑PFAS ranging from 82% to 91% removal rate (Fig. 2a). Although the sum removals were similar across all dosages, the highest magnitude of removal (~91% for ∑PFAS) was observed for 100 g L^{-1} ABR, which aligns with the assumption that higher dosages will provide more available adsorbable sites. For individual PFAS, long-chain compounds showed near-complete to complete removal, whereas short-chain PFAS showed relatively lower removals (Fig. 2a). These trends are consistent with findings from other studies that reported improvements in sorption for PFAS with longer C–F chain length in (i) natural media (*e.g.*, soil and wastewater treatment sludge),[44] (ii) polymeric materials (*e.g.*, polyaniline nanotubes and molecularly imprinted polymers),[45] and (iii) other carbon based-sorbents (*e.g.*, activated carbon and carbon nanotubes).[46] PFAS are amphiphilic substances with hydrophobic per- or polyfluorinated segments and hydrophilic functional groups (*e.g.*, carboxylates, sulfonates). As chain length increases, the hydrophobicity also increases due to the longer aliphatic backbone that can enhance PFAS hydrophobic properties.[2,47] Overall, these hydrophobic interactions improve the affinity of PFAS for the binding sites on each of the adsorbents.[47]

Electrostatic interactions may also play a role in PFAS adsorption by ABR. The PFAS mixture in this study has carboxylic and sulfonate functional groups, which impart a negative charge to the molecules at environmental pH conditions (pK_a ranging from −3.31 to 0.4). This negative charge may then lead to electrostatic repulsions between the

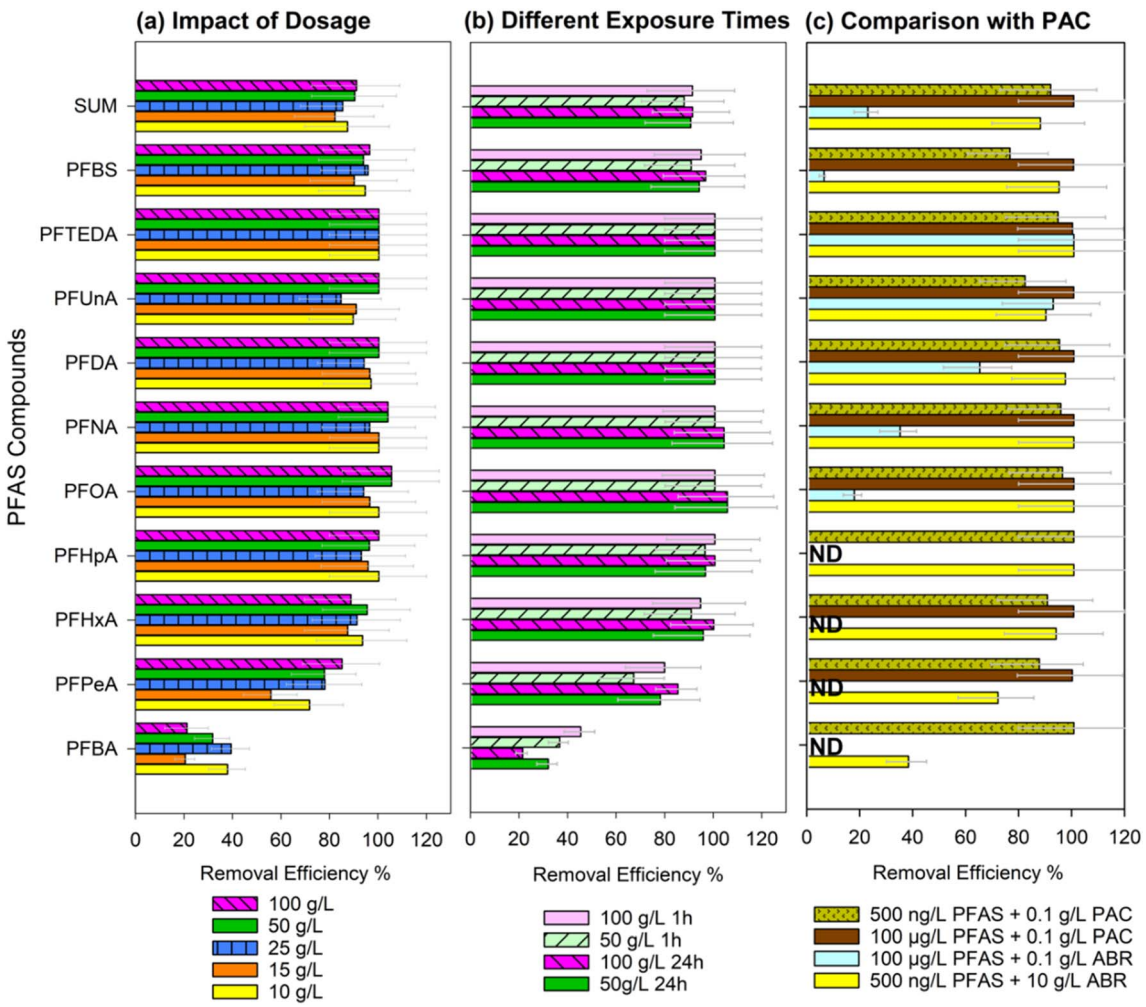

Fig. 2 Removal efficiency of PFAS (a) treated by ABR at various dosages (10–100 g L^{-1}); (b) treated by ABR at various exposure/treatment periods (24 h *vs.* 1 h); and (c) comparison of removal efficiency of PFAS treated by PAC and ABR. Complete substance names and other characteristics are found in Table 1. The "SUM" concentrations represent the total concentrations present in the aqueous phase after the batch adsorption experiment. The error bars represent ±20% measurement uncertainty (typical for trace organic contaminant analysis). The removal efficiency calculation utilized the measured value as the initial concentration instead of the nominal concentration. The reported PFAS concentrations and analytical recoveries can be found in Table S4. ND = not detected.

negatively charged ABR (zeta potential of −6.68 mv at pH 7) and PFAS, but these may have been mitigated by more dominant hydrophobic interactions, especially for the long-chain ones.[46] By contrast, short-chain PFAS are more soluble (due to shorter carbon backbones) and are more likely to be influenced by electrostatic attraction or repulsion.[48] As can be observed here, electrostatic repulsion is likely greater for PFBA (#C = 4) than those with C > 7, which can explain its relatively poor removal by ABR. Despite this, ABR still shows some ability to remove short-chain PFAS (Fig. 2a), suggesting that the positive charges present on the ABR surface can promote some electrostatic attraction, particularly for these smaller, more polar PFAS compounds. As mentioned previously, long-chain PFAS also have a preference to form molecular/colloidal aggregates in the adsorbent surface pores.[37] Their large molecular weights enable adsorbate–adsorbate interactions that eventually form micelle/hemimicelle (small aggregates).[48,49] This further suggests that cooperative adsorption is at play and may be a contributing factor to overall PFAS adsorption to adsorbents.

Our batch experiments further indicate that both short- (1 h) or long-term (24 h) exposure periods were effective for removing long-chain PFAS (~100% removal) (Fig. 2b) and also suggest that equilibrium adsorption could be reached relatively quickly (potentially <1 h for some). However, a longer adsorption period may be required to maximize the removal of short-chain PFAS such as PFPeA. For PFBA, however, lower removals were observed during the 24 h sorption period compared to 1 h experiments. Similar findings were reported by Nakazawa *et al.*, where they observed PFBA desorption from a granular activated carbon (GAC) filter operated at full-scale at a drinking water treatment plant.[50] Many suggest that the formation of small aggregates by long-chain PFAS can displace the already adsorbed short-chain PFAS, eventually leading to the desorption of small-chain PFAS from the adsorbents.[37,48,49]

Additional experiments comparing the performance of a commercially available PAC with ABR showed that for the same initial PFAS concentration (500 ng L^{-1}), the removal efficiency of 10 g L^{-1} ABR was comparable to that of 0.1 g L^{-1} PAC (Fig. 2c). When ABR dosage was lowered to 0.1 g L^{-1}, very low removals were observed for individual and ∑PFAS. This result supports our preliminary hypothesis that, to match the performance of commercially available adsorbents such as activated carbon, larger dosages are required due to ABR's lower surface area.

3.3 PFAS adsorption kinetics and isotherms

3.3.1 Adsorption kinetics. Only 5 of 10 PFAS could be fitted to the adsorption kinetic models as the other substances (PFBA, PFHpA, PFDA, PFUnA, PFTEDA) were already found to be <DL within the first five minutes (Table S5). The rapid decrease in their aqueous phase concentrations may be due their quick adsorption to ABR (*e.g.*, PFDA and PFUnA), high volatility (*e.g.*, PFBA and PFHpA),[51] and loss during the storage/transportation (*e.g.*, PFTEDA). Specifically, PFBA and PFHpA were already < DLs at the start of the experiment (t = 0 min). Although PFDA and PFUnA were at their nominal aqueous phase concentrations (90–100 μg L^{-1}) at t = 0 min, the concentrations were <DL by t = 5 min. For the remaining substances, the kinetic experiments suggest that equilibrium was reached between 5 and 60 min (Fig. 3a). As observed in earlier experiments (Fig. 2a and b), the longer-chain PFAS achieved high removals (~100%) in a relatively short period (within 5–10 min, Fig. 3a). The kinetic study results (Table S6) further indicate that adsorption of PFAS by ABR could be described by either pseudo-first-order (PFO) or pseudo-second-order (PSO) kinetic models (Fig. 3b and c), with PSO fitting the experimental data slightly better (R^2 from 0.995 to 0.999, Table S6). The PSO adsorption rate constant (K_2) ranged from 0.065–5.691 g (μg min)$^{-1}$, with the shortest (PFBS) and longest chain (PFNA) showing the lowest and highest values, respectively (Table S6). The equilibrium adsorption

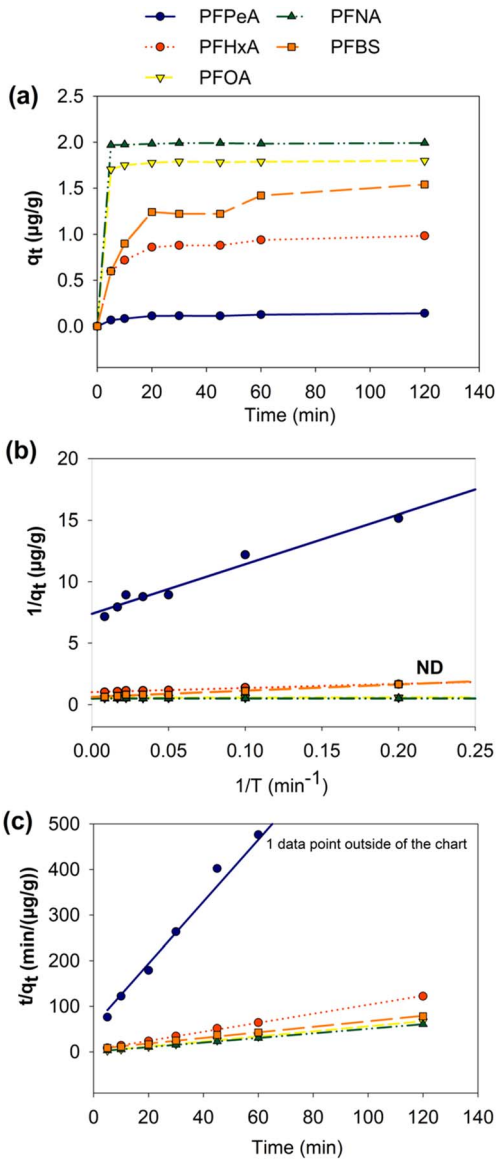

Fig. 3 (a) Concentration of adsorbed PFAS substances obtained during the kinetic study; (b) fitting of the experimental data to pseudo-first-order model; and (c) fitting of the experimental data to pseudo-second-order model.

capacity did not vary widely among PFHxA, PFOA, PFNA, and PFBS (1.012–1.992 μg g^{-1}) but PFPeA was found to have lower adsorption capacity for ABR (0.147 μg g^{-1}). Note that while data were also fitted to intraparticle diffusion kinetic and Elovich models, they did not produce satisfactory results (Table S6).

In general, a PSO model assumes low initial concentration, abundant active sites for the adsorbate, and adsorbates react with adsorbents irreversibly.[52] Irreversibility is of importance to ensure recirculation of PFAS back into the treated wastewater is avoided. Given that chemisorption involves higher energy interactions than physisorption,[53] binding of these five PFAS to ABR is therefore stable. Potential chemisorptive processes are illustrated further by the presence of metal–F bonds on the ABR surface after adsorption (XPS, see Section 3.1). Although it cannot be determined exactly what types of metal–F bonds were formed, it can be hypothesized that PFAS molecules can interact with the metallic elements/oxides present in ABR.

3.3.2 Adsorption isotherm study of PFAS by ABR. Out of the 10 PFAS in the mixture, only 6 could be fitted to adsorption isotherm models, with substances exhibiting different best-fit models (Fig. 4). For instance, PFNA fit the Langmuir model well (R^2 of 0.977) whereas PFHxA and PFHpA followed the Freundlich model (R^2 of 0.966 and 0.998 respectively). PFOA and PFBS were best represented by the Sips model (R^2 of 0.982 and 0.972 respectively), but Langmuir and Freundlich may also apply (R^2 of 0.963 and 0.950 for PFOA; 0.802 and 0.915 for PFBS respectively) (Table 4). None of the substances fit the Toth model.

Although the goodness-of-fit is a good metric for isotherm model choice, others caution choosing the isotherm solely on this criterion as it may not always provide meaningful or practical insights.[53,54] For instance, the heterogenicity of ABR surface and potential aggregation of PFAS during adsorption[49,55] conflict with the monolayer assumption of the Langmuir model. Hence, although PFNA fit well *via* Langmuir, Freundlich isotherm (multi-layer adsorption) is more applicable despite the lower R^2 value (*i.e.*, 0.977 *vs.* 0.881). Additionally, since PFAS adsorption follows the PSO kinetic model which implies irreversibility challenges the choice of Langmuir model where reactions are assumed to be reversible.[53]

As for Freundlich isotherm, the $1/n$ value provides insights related to the adsorption mechanism, where a value of $1/n > 1$ indicates that additional sorbates are bound to the adsorbent by weaker and weaker free energies.[56] As an indicative of affinity, $1/n > 1$ also suggests that the adsorption tendency increased as the surface concentration of PFAS increased.[56,57] Therefore, the cooperative adsorption among the adsorbates is an important mechanism for substances behaving this way (*i.e.*, sorbed

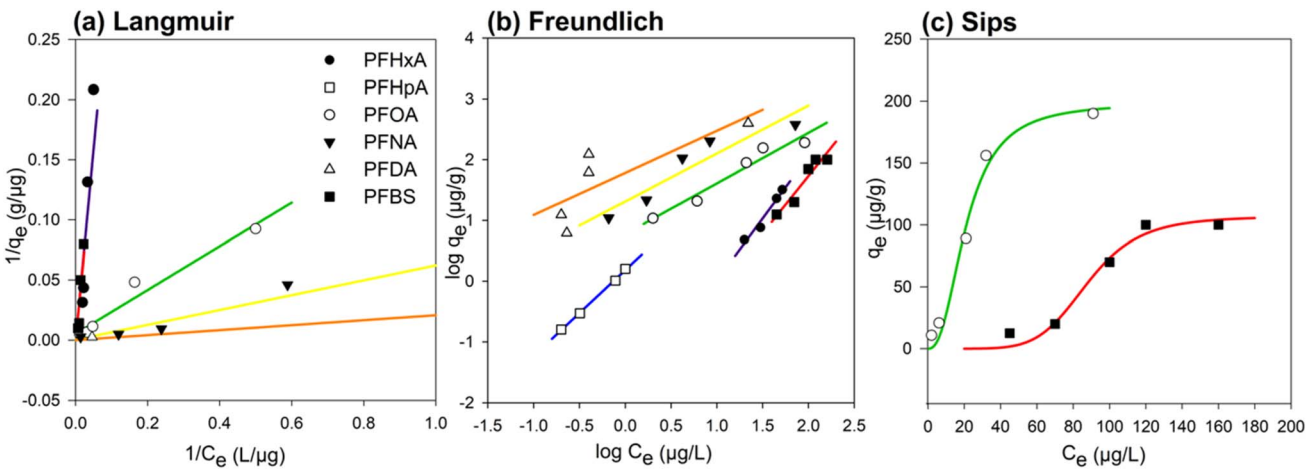

Fig. 4 The adsorption isotherm for PFAS by ABR fitting *via* (a) Langmuir, (b) Freundlich, and (c) Sips isotherm model based on equilibrium concentrations derived dosages ranging from 0.1 to 10 g L^{-1}.

Table 4 Adsorption isotherm parameters obtained for the removal of PFAS. Q_m (μg g^{-1}) = adsorption capacity for each model; K_L (L g^{-1}) = the isotherm constant for the Langmuir model; K_F = the isotherm constant for the Freundlich model; $1/n$ = the constant for the Freundlich model; K_S = the isotherm constant for the Sips model; b = intercept for Sips model. None of PFAS followed the Toth model

	Langmuir			Freundlich			Sips			
PFAS	K_L (L μg^{-1})	Q_m (μg g^{-1})	R^2	K_F	$1/n$	R^2	K_S	b	Q_m (μg g^{-1})	R^2
PFHxA	0	4.11×10^{11}	0.515	0.009	2.050	0.966	—			
PFHpA	—			1.523	1.416	0.998	—			
PFOA	0.029	188.679	0.963	5.958	0.834	0.950	0.001	2.433	198.793	0.982
PFNA	0.005	3333.333	0.977	20.469	0.791	0.881	—			
PFDA	0	5.380×10^{9}	0.523	60.632	0.693	0.641	—			
PFBS	0	2.288×10^{12}	0.802	0.009	1.887	0.915	1.24×10^{-12}	6.123	106.729	0.973

sorbates bring in more sorbates *via* attractive interactions). This aligns with the assumption that the interactions between PFAS molecules can create micelle/hemimicelle formation (*i.e.*, surfactant aggregates),[37,39,40] further influencing their multilayer adsorption on adsorbents.

Sips model is a hybrid of Langmuir and Freundlich (mathematically) and can represent adsorption equilibrium for a wide range of adsorbate concentrations, whether the surface is homogeneous or heterogeneous.[53] The good fit of experimental data to Sips model also indicates PFOA adsorption on ABR can reduce to the Freundlich isotherm as the concentration decreases.[55]

Important information derived from isotherm experiments is the maximum adsorption capacity (Q_m) of the material (for Langmuir and Sips), and the opportunity to determine the desired dosage of adsorbent when operated in a completely mixed flow reactor system (CMFR) (for the case of Freundlich isotherm). This is illustrated in eqn (S13) and (S14), and depending on the target removal requirements, the ABR dose to reach the target efficiency could be estimated. For instance, to remove 50–95% of PFHpA *via* ABR, doses ranging from 0.1 to 6.4 g L^{-1} are required (Table S6). From here, it appears that a concentration of up to 10 g L^{-1} ABR is suitable to remove most of the substances (ΣPFAS removal of >85%), substantially reducing the ABR dosage from earlier experiments (100 g L^{-1}).

3.4 Cytotoxicity assessment of ABR treatment

A prior study from our group suggested that ABR toxicity and leaching of trace metals can be mitigated by adjusting pH to ~7.[28] Although pH adjustment was completed during the experiments, we still deemed it important to track toxicities at various dosages. Cytotoxicity *via* the *Aliivibrio fisheri* shows different toxicity behaviours at various concentrations and dosages (Fig. 5). Cytotoxicity decreased upon the addition of ABR at 10 g L^{-1} compared to 0 g L^{-1} ABR (*i.e.*, PFAS only), increased at 50 g L^{-1} and finally dropped to background levels at 100 g L^{-1} dosage. This observation was similar to a prior toxicity assessment of ABR at these dosages.[28]

Although it was observed here that PFAS removals were improved at higher ABR dosages (Fig. 2a), the result further suggests that there is a potential for increased toxicity at higher dosages. Hence, the results support the use of <10 g L^{-1} ABR dosage as suggested from the isotherm data (see Section 3.3) as both removal efficiency is maximized, and the potential toxicity is minimized. This result is also useful for future ABR operation as cytotoxicity can be tracked and compared to effects-based trigger values for ecosystem protection should the treated water be discharged into a receiving environment (*i.e.* if $1/IC10_{REF} < 20$ after dilution is considered). If this is not possible, further material modification (*e.g.*, heat or acid treatment) may be required to reduce toxicity.

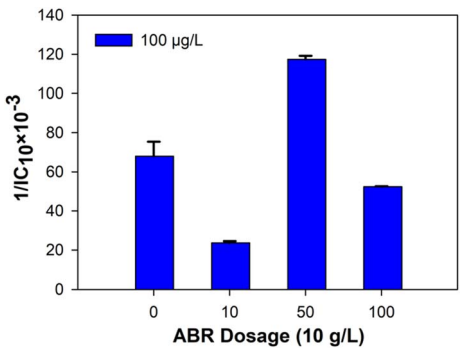

Fig. 5 $1/IC_{10REF}$ of samples after treatment with different dosages of ABR.

3.5 Additional insights into ABR treatment

A main disadvantage of ABR against commercially available adsorbents (PAC or GAC) is its relatively low porosity and therefore requires a higher dosage to achieve the same removal. Also, this study only assessed the removals of PFAS in ultrapure water. Though the result of the isotherm study suggested 10 g L^{-1} of ABR is enough to remove most PFAS in a "PFAS-only" system, other organic substances (natural [*e.g.*, humic acids] and synthetic ones [*e.g.*, trace organic substances such as pharmaceuticals]) and inorganic anions (*e.g.*, SO_4^{2-}) may also be present. Hence, low dosage of ABR may not be applicable as a result of competitive sorption and therefore must be explored. In recent years, the reuse of industrial solid waste has gained attention as a strategy to achieve the globally recognized sustainable development goals (SDGs).[58,59] The sharp increase in global waste generation has imposed considerable stress on the environment, necessitating innovative and sustainable solutions.[60] The source material for ABR is found in large amounts (3–4 billion MT global stockpile)[61] and can be easily accessed and utilized. The global demand for aluminum will only grow, suggesting that alumina extraction from bauxite deposits will increase the waste associated with this process. Therefore, the utilization of various waste materials for waste treatment processes (*e.g.*, wastewater remediation) offers a sustainable pathway.[59,62] The reuse of bauxite residue as an adsorbent material to remove PFAS from wastewater presents a promising approach to closing material loops in a more economical and less hazardous way. More specifically, we envision ABR as a polishing step in wastewater treatment as its impact on biological processes is currently unknown. It is also important to minimize secondary risks of pollution. Although we have shown that neutralization (pH adjustment to ~7) reduces toxicity and leaching of ABR-bound metals at bench-scale, this must be tested at a pilot- or larger-scale. In terms of managing the spent ABR, more work on the material regeneration and PFAS destruction is required (*e.g.*, *via* thermal treatment).

4 Conclusion

This study investigated the feasibility of ABR as a potential adsorbent material to remove PFAS from the water column. ABR was characterized as a porous and charged material with heterogeneous mesopores. After being over-saturated with PFAS, ABR characterization revealed the presence of fluorine

atoms along with C–F and metal–F bonds on the surface. The decreasing PZC of spent ABR indicated that neutral conditions can help maximize the adsorption of PFAS. Our results further showed the removal efficiency of 10 g L^{-1} ABR was acceptable for $\sum$PFAS and comparable to that of 0.1 g L^{-1} PAC. However, short-chain PFAS cannot be completely removed, and the dosage of ABR cannot be further lowered to the same level as the commercially available PAC. Furthermore, the adsorption of PFAS followed the PSO kinetics, suggesting chemisorption might be the dominant adsorption mechanism combined with the appearance of metal–F bonds. Adsorption isotherm studies provided the potential to remove most PFAS using up to 10 g L^{-1} ABR. Moreover, ABR effectively removed cytotoxicity introduced by PFAS at 10 g L^{-1}, but higher dosages will likely introduce more toxicity given ABR's known toxic potential.

In the future, further improvements in ABR characteristics can be made, and optimization of ABR dosage and treatment conditions can be assessed on a pilot- or full-scale and promote the comprehensive evaluation of the combination of ABR with existing WWTP processes. Finally, spent ABR (*i.e.*, after wastewater treatment) allows for the extraction of metals and subsequent reuse processes (*e.g.*, construction material/roadway aggregates). Given the large amounts of source material and ABR use, there is a potential for ABR to be utilized as an economically and environmentally friendly adsorbent material to remove PFAS and as a supplement to the existing treatment process.

Conflicts of interest

There are no conflicts to declare.

Data availability

Raw data will be made available upon request.

The processed data supporting this article have been included as part of the supplementary information (SI). Supplementary information: pre-experiment preparations, material specification and characterization, equations used within the article, PFAS concentration data, and optimal dosage calculations. See DOI: **https://doi.org/10.1039/d5va00101c**.

Acknowledgements

This work was financially supported by Mitacs Accelerate (75%) and GRÖN Holding Corp. (25%). Additional funding from the NSERC Discovery Grant (NSERC RGPIN-2021-02412) was also obtained to support this work. We also gratefully acknowledge the help and support of the NanoFAB facility from the University of Alberta.

References

1 C. Gallen, G. Eaglesham, D. Drage, T. H. Nguyen and J. F. Mueller, A mass estimate of perfluoroalkyl substance (PFAS) release from Australian wastewater treatment plants, *Chemosphere*, 2018, **208**, 975–983.

2 Z. Du, S. Deng, Y. Bei, Q. Huang, B. Wang, J. Huang, *et al.*, Adsorption behavior and mechanism of perfluorinated compounds on various adsorbents—A review, *J. Hazard. Mater.*, 2014, **274**, 443–454.

3 J. Glüge, M. T. Scheringer, I. Cousins, C. DeWitt J, G. Goldenman, D. Herzke, *et al.*, An overview of the uses of per- and polyfluoroalkyl substances (PFAS), *Environ. Sci.: Processes Impacts*, 2020, **22**(12), 2345–2373.

4 R. Lohmann, I. T. Cousins, J. C. DeWitt, J. Glüge, G. Goldenman, D. Herzke, *et al.*, Are Fluoropolymers Really of Low Concern for Human and Environmental Health and Separate from Other PFAS?, *Environ. Sci. Technol.*, 2020, **54**(20), 12820–12828.

5 S. P. Lenka, M. Kah and L. P. Padhye, A review of the occurrence, transformation, and removal of poly- and perfluoroalkyl substances (PFAS) in wastewater treatment plants, *Water Res.*, 2021, **199**, 117187.

6 Z. Abunada, M. Y. D. Alazaiza and M. J. K. Bashir, An Overview of Per- and Polyfluoroalkyl Substances (PFAS) in the Environment: Source, Fate, Risk and Regulations, *Water*, 2020, **12**(12), 3590.

7 O. S. Arvaniti, Y. Hwang, H. R. Andersen, A. S. Stasinakis, N. S. Thomaidis and M. Aloupi, Reductive degradation of perfluorinated compounds in water using Mg-aminoclay coated nanoscale zero valent iron, *Chem. Eng. J.*, 2015, **262**, 133–139.

8 M. Wilhelm, S. Bergmann and H. H. Dieter, Occurrence of perfluorinated compounds (PFCs) in drinking water of North Rhine-Westphalia, Germany and new approach to assess drinking water contamination by shorter-chained C4–C7 PFCs, *Int. J. Hyg. Environ. Health*, 2010, **213**(3), 224–232.

9 State Water Resources Control Board Division of Water Quality GAMA Program, in *GROUNDWATER INFORMATION SHEET Perfluorooctanoic Acid (PFOA) & Perfluorooctanesulfonic Acid (PFOS)*, 2019.

10 D. M. Wanninayake, Comparison of currently available PFAS remediation technologies in water: A review, *J. Environ. Manage.*, 2021, **283**, 111977.

11 H. Hamid and L. Li, Role of wastewater treatment plant in environmental cycling of poly- and perfluoroalkyl substances, *Ecocycles*, 2016, **2**(2), 43–53.

12 P. Guerra, M. Kim, L. Kinsman, T. Ng, M. Alaee and S. A. Smyth, Parameters affecting the formation of perfluoroalkyl acids during wastewater treatment, *J. Hazard. Mater.*, 2014, **272**, 148–154.

13 M. Faysal Hossain, N. Akther and Y. Zhou, Recent advancements in graphene adsorbents for wastewater treatment: Current status and challenges, *Chin. Chem. Lett.*, 2020, **31**(10), 2525–2538.

14 A. A. Siyal, M. R. Shamsuddin, A. Low and N. E. Rabat, A review on recent developments in the adsorption of surfactants from wastewater, *J. Environ. Manage.*, 2020, **254**, 109797.

15 W. Chen, X. Zhang, M. Mamadiev and Z. Wang, Sorption of perfluorooctane sulfonate and perfluorooctanoate on polyacrylonitrile fiber-derived activated carbon fibers: in

comparison with activated carbon, *RSC Adv.*, 2017, **7**(2), 927–938.
16 Y. Yang, Z. Zheng, W. Ji, J. Xu and X. Zhang, Insights to perfluorooctanoic acid adsorption micro-mechanism over Fe-based metal organic frameworks: Combining computational calculation with response surface methodology, *J. Hazard. Mater.*, 2020, **395**, 122686.
17 R. Li, S. Alomari, R. Stanton, M. C. Wasson, T. Islamoglu, O. K. Farha, *et al.*, Efficient Removal of Per- and Polyfluoroalkyl Substances from Water with Zirconium-Based Metal–Organic Frameworks, *Chem. Mater.*, 2021, **33**(9), 3276–3285.
18 A. Zaggia, L. Conte, L. Falletti, M. Fant and A. Chiorboli, Use of strong anion exchange resins for the removal of perfluoroalkylated substances from contaminated drinking water in batch and continuous pilot plants, *Water Res.*, 2016, **91**, 137–146.
19 S. Rai, S. Bahadure, M. J. Chaddha and A. Agnihotri, A Way Forward in Waste Management of Red Mud/Bauxite Residue in Building and Construction Industry, *Trans Indian Natl Acad Eng*, 2020, **5**(3), 437–448.
20 S. Alam, S. Jain and S. K. Das, inCharacterization and an Overview of Utilization and Neutralization for Efficient Management of Bauxite Residue for Sustainable Environment, ed. Achal V. and Chin C. S., *Building Materials for Sustainable and Ecological Environment*, Singapore, Springer, 2021, pp. 25–47, DOI: **10.1007/978-981-16-1706-5_3**.
21 K. Evans, The History, Challenges, and New Developments in the Management and Use of Bauxite Residue, *J. Sustain. Metall.*, 2016, **2**(4), 316–331.
22 I. Panda, S. Jain, S. K. Das and R. Jayabalan, Characterization of red mud as a structural fill and embankment material using bioremediation, *Int. Biodeterior. Biodegrad.*, 2017, **119**, 368–376.
23 S. Rai, S. Bahadure, M. J. Chaddha and A. Agnihotri, Disposal Practices and Utilization of Red Mud (Bauxite Residue): A Review in Indian Context and Abroad, *J. Sustain. Metall.*, 2020, **6**(1), 1–8.
24 M. C. Mishra, N. Gangadhara Reddy, R. B. Hanumantha and S. Kumar Das, in A Study on Evaluating the Usefulness and Applicability of Additives for Neutralizing Extremely Alkaline Red Mud Waste, ed. Reddy K. R., Agnihotri A. K., Yukselen-Aksoy Y., Dubey B. K. and Bansal A., *Sustainable Environmental Geotechnics*. Cham, Springer International Publishing, 2020. pp. 139–49.
25 L. Wang, G. Hu, F. Lyu, T. Yue, H. Tang, H. Han, *et al.*, Application of Red Mud in Wastewater Treatment, *Minerals*, 2019, **9**(5), 281.
26 S. Rai, S. Bahadure, M. J. Chaddha and A. Agnihotri, in Utilization of Aluminium Industry Solid Waste (Red Mud/Bauxite Residue) in Pollution Control, ed. Randive K., Pingle S. and Agnihotri A., *Innovations in Sustainable Mining: Balancing Environment, Ecology and Economy*, Cham, Springer International Publishing, 2021, pp. 21–43. DOI: **10.1007/978-3-030-73796-2_2**.
27 M. Habuda-Stanić, M. E. Ravančić and A. Flanagan, A Review on Adsorption of Fluoride from Aqueous Solution, *Materials*, 2014, **7**(9), 6317–6366.
28 F. Cheng, J. Pang, S. Berggren, H. Tanvar, B. Mishra and M. J. Arlos, Treating Waste with Waste: Activated Bauxite Residue (ABR) as a Potential Wastewater Treatment, *ACS Omega*, 2024, **9**(45), 45251–45262.
29 A. Bhatnagar, V. J. P. Vilar, C. M. S. Botelho and R. A. R. Boaventura, A review of the use of red mud as adsorbent for the removal of toxic pollutants from water and wastewater, *Environ. Technol.*, 2011, **32**(3), 231–249.
30 B. A. Mohamed, X. Bi, L. Y. Li, L. Leng, E. S. Salama and H. Zhou, Bauxite residue as a catalyst for microwave-assisted pyrolysis of switchgrass to high quality bio-oil and biochar, *Chem. Eng. J.*, 2021, **426**, 131294.
31 X. Qi, H. Wang, C. Huang, L. Zhang, J. Zhang, B. Xu, *et al.*, Analysis of bauxite residue components responsible for copper removal and related reaction products, *Chemosphere*, 2018, **207**, 209–217.
32 S. Gostu. Investigation of carbon-based reductant, low-temperature process for conversion of hematite in red-mud to magnetite - ProQuest. 2016**https://www.proquest.com/docview/1766582114?pq-origsite=gscholar&fromopenview=true&sourcetype=Dissertations%20&%20Theses**.
33 K. I. Barrow, B. A. Escher, K. Hicks, M. König, R. Schlichting and J. Arlos M, Water quality monitoring with *in vitro* bioassays to compare untreated oil sands process-affected water with unimpacted rivers, *Environ. Sci.:Water Res. Technol.*, 2023, **9**(8), 2008–2020.
34 C. Pelekani and V. L. Snoeyink, Competitive adsorption in natural water: role of activated carbon pore size, *Water Res.*, 1999, **33**(5), 1209–1219.
35 M. Thommes, K. Kaneko, A. V. Neimark, J. P. Olivier, F. Rodriguez-Reinoso, J. Rouquerol, *et al.*, Physisorption of gases, with special reference to the evaluation of surface area and pore size distribution (IUPAC Technical Report), *Pure Appl. Chem.*, 2015, **87**(9–10), 1051–1069.
36 P. Punyapalakul, K. Suksomboon, P. Prarat and S. Khaodhiar, Effects of Surface Functional Groups and Porous Structures on Adsorption and Recovery of Perfluorinated Compounds by Inorganic Porous Silicas, *Sep. Sci. Technol.*, 2013, **48**(5), 775–788.
37 E. Gagliano, M. Sgroi, P. P. Falciglia, F. G. A. Vagliasindi and P. Roccaro, Removal of poly- and perfluoroalkyl substances (PFAS) from water by adsorption: Role of PFAS chain length, effect of organic matter and challenges in adsorbent regeneration, *Water Res.*, 2020, **171**, 115381.
38 L. Li, P. A. Quinlivan and D. R. U. Knappe, Effects of activated carbon surface chemistry and pore structure on the adsorption of organic contaminants from aqueous solution, *Carbon*, 2002, **40**(12), 2085–2100.
39 P. Kingshott, G. Andersson, S. L. McArthur and H. J. Griesser, Surface modification and chemical surface analysis of biomaterials, *Curr. Opin. Chem. Biol.*, 2011, **15**(5), 667–676.

40 J. Lefebvre, F. Galli, C. L. Bianchi, G. S. Patience and D. C. Boffito, Experimental methods in chemical engineering: X-ray photoelectron spectroscopy-XPS, *Can. J. Chem. Eng.*, 2019, **97**(10), 2588–2593.

41 V. Presser, C. Berthold, R. Wirth and K. G. Nickel, Structural characterisation of tribologically influenced silicon carbide ceramic surfaces, *Curr. Opin. Solid State Mater. Sci.*, 2008, **12**(5), 73–80.

42 I. Murrieta-Pazos, C. Gaiani, L. Galet, B. Cuq, S. Desobry and J. Scher, Comparative study of particle structure evolution during water sorption: Skim and whole milk powders, *Colloids Surf., B*, 2011, **87**(1), 1–10.

43 J. Wang, Z. Lin, X. He, M. Song, P. Westerhoff, K. Doudrick, *et al.*, Critical Review of Thermal Decomposition of Per- and Polyfluoroalkyl Substances: Mechanisms and Implications for Thermal Treatment Processes, *Environ. Sci. Technol.*, 2022, **56**(9), 5355–5370.

44 O. S. Arvaniti, H. R. Andersen, N. S. Thomaidis and A. S. Stasinakis, Sorption of Perfluorinated Compounds onto different types of sewage sludge and assessment of its importance during wastewater treatment, *Chemosphere*, 2014, **111**, 405–411.

45 F. Cao, L. Wang, X. Ren and H. Sun, Synthesis of a perfluorooctanoic acid molecularly imprinted polymer for the selective removal of perfluorooctanoic acid in an aqueous environment, *J. Appl. Polym. Sci.*, 2016, **133**(15), DOI: **10.1002/app.43192**.

46 H. Smaili and C. Ng, Adsorption as a remediation technology for short-chain per- and polyfluoroalkyl substances (PFAS) from water – a critical review, *Environ. Sci.:Water Res. Technol.*, 2023, **9**(2), 344–362.

47 M. Park, S. Wu, I. J. Lopez, J. Y. Chang, T. Karanfil and S. A. Snyder, Adsorption of perfluoroalkyl substances (PFAS) in groundwater by granular activated carbons: Roles of hydrophobicity of PFAS and carbon characteristics, *Water Res.*, 2020, **170**, 115364.

48 Vu C. Thanh and T. Wu, Adsorption of short-chain perfluoroalkyl acids (PFAAs) from water/wastewater, *Environ. Sci.:Water Res. Technol.*, 2020, **6**(11), 2958–2972.

49 P. McCleaf, S. Englund, A. Östlund, K. Lindegren, K. Wiberg and L. Ahrens, Removal efficiency of multiple poly- and perfluoroalkyl substances (PFASs) in drinking water using granular activated carbon (GAC) and anion exchange (AE) column tests, *Water Res.*, 2017, **120**, 77–87.

50 Y. Nakazawa, K. Kosaka, M. Asami and Y. Matsui, Maximum desorption of perfluoroalkyl substances adsorbed on granular activated carbon used in full-scale drinking water treatment plants, *Water Res.*, 2024, **254**, 121396.

51 PhysChemProp_Table_July2023-FINAL.xlsx, available from: **https://view.officeapps.live.com/op/view.aspx?src=https%3A%2F%2Fpfas-1.itrcweb.org%2Fwp-content%2Fuploads%2F2022%2F01%2FPhysChemProp_Table_July2023-FINAL.xlsx&wdOrigin=BROWSELINK**.

52 Y. Wang, C. Wang, X. Huang, Q. Zhang, T. Wang and X. Guo, Guideline for modeling solid-liquid adsorption: Kinetics, isotherm, fixed bed, and thermodynamics, *Chemosphere*, 2024, **349**, 140736.

53 J. Plazas-Tuttle, F. M. Giraldo and A. Avila. *Nanomaterials for the Detection and Removal of Wastewater Pollutants*. Elsevier; 2020, available from: **https://linkinghub.elsevier.com/retrieve/pii/B9780128184899000013**.

54 K. D. Hristovski and J. Markovski, Engineering metal (hydr) oxide sorbents for removal of arsenate and similar weak-acid oxyanion contaminants: A critical review with emphasis on factors governing sorption processes, *Sci. Total Environ.*, 2017, **598**, 258–271.

55 N. Tzabar and H. J. M. ter Brake, Adsorption isotherms and Sips models of nitrogen, methane, ethane, and propane on commercial activated carbons and polyvinylidene chloride, *Adsorption*, 2016, **22**(7), 901–914.

56 R. P. Schwarzenbach, P. M. Gschwend and D. M. Imboden. *Environmental Organic Chemistry*. John Wiley & Sons; 2016. p. 1026.

57 X. Chen, M. F. Hossain, C. Duan, J. Lu, Y. F. Tsang, M. S. Islam, *et al.*, Isotherm models for adsorption of heavy metals from water - A review, *Chemosphere*, 2022, **307**, 135545.

58 K. Obaideen, N. Shehata, E. T. Sayed, M. A. Abdelkareem, M. S. Mahmoud and A. G. Olabi, The role of wastewater treatment in achieving sustainable development goals (SDGs) and sustainability guideline, *Energy Nexus*, 2022, (7), 100112.

59 N. Karić, A. S. Maia, A. Teodorović, N. Atanasova, G. Langergraber, G. Crini, *et al.*, Bio-waste valorisation: Agricultural wastes as biosorbents for removal of (in) organic pollutants in wastewater treatment, *Chem. Eng. J. Adv.*, 2022, **9**, 100239.

60 X. Peng, Y. Jiang, Z. Chen, A. I. Osman, M. Farghali, D. W. Rooney, *et al.*, Recycling municipal, agricultural and industrial waste into energy, fertilizers, food and construction materials, and economic feasibility: a review, *Environ. Chem. Lett.*, 2023, **21**(2), 765–801.

61 R. Khanna, Y. Konyukhov, D. Zinoveev, K. Jayasankar, I. Burmistrov, M. Kravchenko, *et al.*, Red Mud as a Secondary Resource of Low-Grade Iron: A Global Perspective, *Sustainability*, 2022, **14**(3), 1258.

62 N. H. Solangi, J. Kumar, S. A. Mazari, S. Ahmed, N. Fatima and N. M. Mubarak, Development of fruit waste derived bio-adsorbents for wastewater treatment: A review, *J. Hazard. Mater.*, 2021, **416**, 125848.